



Technical note

Fixed-order gain-scheduling anti-sway control of overhead bridge cranes

Michele Ermidoro^{a,*}, Alberto L. Cologni^a, Simone Formentin^b, Fabio Previdi^a^a Dipartimento di ingegneria e scienze applicate, Università degli studi di Bergamo, Italy^b Dipartimento di Elettronica e Informazione, Politecnico di Milano, Milano, Italy

ARTICLE INFO

Article history:

Received 13 October 2015

Revised 20 June 2016

Accepted 26 June 2016

Available online 5 July 2016

Keywords:

Gain-scheduling

Fixed-order controller

Bridge cranes

ABSTRACT

Acceleration and deceleration in overhead cranes may induce undesirable load swinging, which is unsafe for the surrounding human operators. In this paper, it is shown that such oscillatory behavior depends on the length of the rope and thus a gain-scheduling control law is proposed to reduce such an effect. Specifically, to take into account the technological limits in the controller implementation, a fixed-order controller is tuned, by also enforcing robustness and performance constraints. The proposed strategy is experimentally tested on a real bridge crane and compared to a time-invariant solution.

© 2016 Elsevier Ltd. All rights reserved.

1. Introduction

In the modern industry, many challenging manipulation tasks with heavy objects are usually handled via overhead cranes. Such cranes can be classified as gantry cranes and bridge cranes. The former are typically used in container terminals and are characterized by the fact that the entire structure is wheeled along the ground. Instead, the bridge cranes, which are more frequently used in the industrial environment, have a fixed supporting structure, while the movable hoist runs overhead along a rail or a beam.

Overhead cranes suffer from safety problems due to the flexibility of the rope linking the load to the hoist. In fact, the load swinging is usually very poorly damped and the uncontrolled sway might be dangerous for human operators. Moreover, the oscillations require a certain time to stop, thus slowing the overall movement time.

Many approaches have been proposed to solve the problem of the load oscillations induced by the movement of the crane. A second order sliding mode control has been used in [4] while in [15] an adaptive sliding mode control is employed. The approaches in [3] and [7] adopt a time optimal perspective, while [18] and [19] propose an open-loop input shaping method.

All the above solutions do not consider the fact that the rope length and the mass of the load may change during the system operation; nevertheless, such events occur quite often

in practical working cycles. For this reason, gain-scheduled controllers appear to be a suited solution to the problem of sway suppression.

Among the solutions addressing the problem at hand from a gain-scheduling perspective, the method in [6] considers the length of the rope as a scheduling signal for an implicit gain scheduling controller and employs the knowledge of the upper bounds in the rate of change of such a parameter to ensure the stability of the closed-loop system. In [20] a state-space interpolation method is used to an analogous design purpose. This method, albeit providing good performance, does not ensure the stability of the systems in case of parameter variations.

In all the above contributions, simplicity and robustness with respect to model uncertainty are not requested as important features of the final control system.

In this paper, the problem of sway cancellation in overhead bridge cranes is tackled from a gain-scheduled rationale, but also taking into account the simplicity of the final controller (to make it suitable for implementation on a wide range of micro-controllers or PLCs) and finding the best trade off between performance and robustness. More specifically, a fixed-order gain scheduling controller is designed (thus with a user-defined structure) aimed to minimize the integral error but also constraining the main robustness margins. The proposed method has been first introduced in [10], but herein the minimization of the settling time is also considered. A secondary aim of this paper is to show why the rope length, and not the load mass, should be used as a scheduling variable.

* Corresponding author.

E-mail addresses: michele.ermidoro@unibg.it (M. Ermidoro), formentin@elet.polimi.it (S. Formentin).

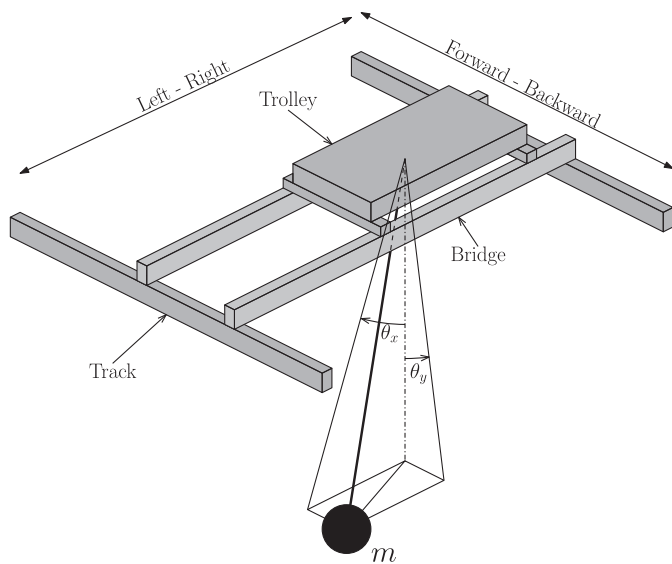


Fig. 1. The typical structure of a bi-dimensional bridge crane. The trolley moves right or left (X axis) on the bridge, which moves forward or backward (Y axis) on the track. The payload is connected to the trolley using a rigid rope and it can swing on both axes.

The fixed-order gain scheduling controller is experimentally implemented on a real bridge crane and the achieved performance is compared to that of a linear time-invariant controller tuned according to the same specifications. The experiments show that, although the employed structure is very simple, the gain scheduling controller is able to suppress the sway in all the conditions of interest, unlike the time-invariant solution. It has to be stressed that, in the proposed closed-loop solution, where the oscillations are estimated through proper measurements and automatically compensated by a feedback controller, the operator can still manually operate the system, without predefining any reference trajectory. Finally, a comparison with well established tools for gain scheduling design shows that similar performance in terms of sway reduction can be achieved, but without requiring any speed feedback and with lower order controllers.

This remainder of the paper is organized as follows. Section 2 describes the experimental setup and the problem statement. In Section 3 the model of the system is derived and experimentally validated. Then, the fixed-order gain-scheduling control design method is described in Section 4, with a focus on how to select the different tuning knobs. Section 5 presents the experimental results, while some remarks end the paper in Section 6.

2. System description and problem statement

The typical setup of a manually operated bridge crane is illustrated in Fig. 1, where the two main components of the system are shown: the bridge, which moves along the Y axis on the track in the given reference framework, and the trolley, which moves along the X axis on the bridge. The cargo is normally suspended on the cable by a hook and can oscillate along any direction. The sway has a detrimental effect on the maneuvering performance and, more worrisome, on the safety of human operators, who manually moves the crane by remote control.

The architecture of the bridge crane, for each axis, is depicted in Fig. 2. The operator, using a button panel, sends commands to the motor and varies the position x and the sway angle ϑ . The oscillation is then controlled by means of a feedback loop.

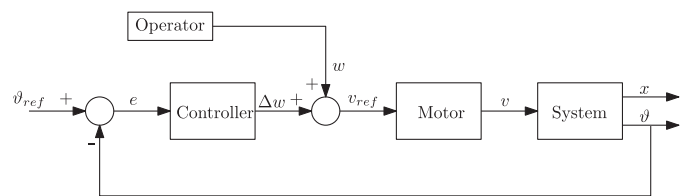


Fig. 2. Block diagram of the system. The operator enters in the loop as a disturb.



Fig. 3. The real bridge crane used for the tests. The X and Y axes are super imposed.

The purpose of the paper is to design a controller which is able to remove the sway without affecting the human/system interaction.

2.1. Experimental setup

The designed controller has been implemented and tested on a real bridge crane, shown in Fig. 3. It has a maximum payload of 20,000 kg and can move on all the three axes. On the X-axis and Y-axis it can move at a maximum speed of 1 m/s while on the Z-axis, it can lift the objects at around 0.2 m/s. The bridge has an elevation from the ground of around 7 m, while the trolley can span for 20 m while the bridge on the Y-axis can move for around 80 m (this distance depends even on the presence of other overhead cranes on the same track).

In order to estimate the oscillation angle, an inertial platform composed by a tri-axial accelerometer and a tri-axial gyroscope has been placed on the rope that connects the load to the trolley. In order to keep the sensor in a safe position it has been placed near the turnbuckle which is the part of the rope that link the cable to the crane, and, consequentially does not move. From the raw measurements the angle is estimated using the Extended Kalman filter described in ([5]).

The raw estimated angle is then acquired by a PLC. This angle is still not suitable for the control purpose, due to some differences between the model described in Section 3. The connection between the load and the trolley is composed by more than one rope and they are not connected perpendicularly to the trolley. For this reason a high pass filter is needed to remove the offset introduced by the connection of the rope to the turnbuckle. Another problem introduced by the ropes is related to their not fully stiffness; in fact this leads to high frequency vibrations of the ropes that can be easily removed using a low pass filter. The PLC then drives an inverter which puts the motor in movement. The actuation chain, from the PLC to the speed of the motor is not ideal; if the bandwidth of the motor controller can be considered wide enough, the delay introduced can not be neglected. This nominal delay has a fixed amount and it is due to the disabling of the brakes.

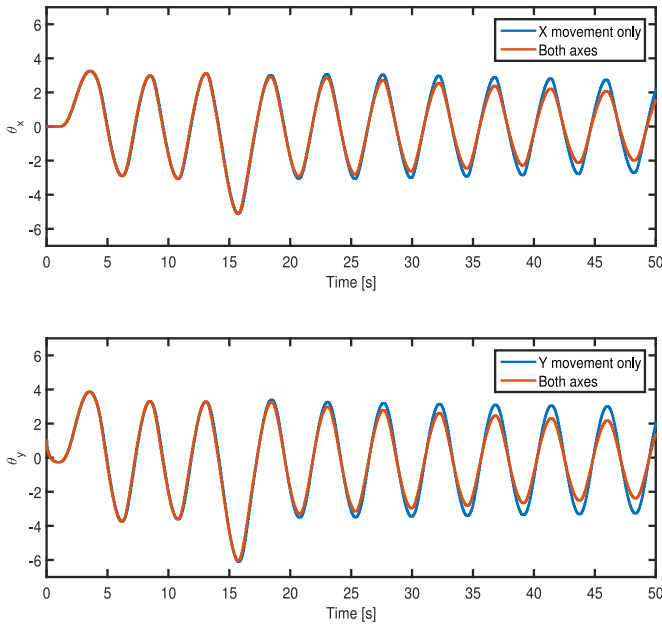


Fig. 4. When the crane is moving along the bridge axis (θ_x), the angle produced on the other axis is negligible and vice-versa, so the dynamics along the two directions can be assumed to be decoupled.

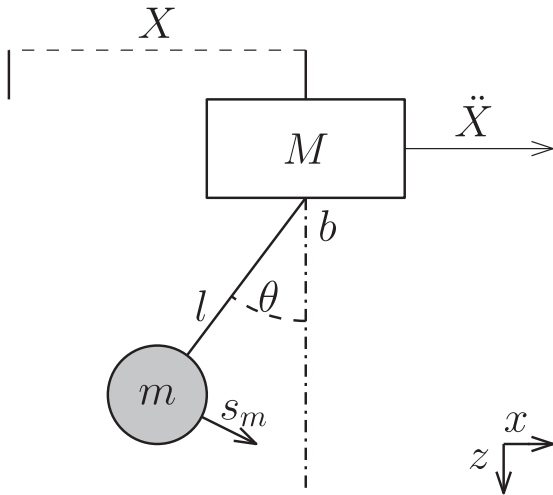


Fig. 5. Structure of a mono-dimensional bridge crane.

3. Modeling

The system is assumed to be completely decoupled as discussed in ([17]), so the model is built for a mono-axial cart-pendulum as the one visible in Fig. 5. The assumption holds true also for our experimental setup. This fact can be easily checked by moving the crane along one axis at a time or both axes at the same time (test in Fig. 4). Notice that, since the mutual effects of the two axes are clearly negligible, x and y can be treated independently.

The control will be then tuned on the identified models on the X and Y axes controlling the sway on both directions. In Fig. 5, $X(t)$ is the position, $\ddot{X}(t)$ is the acceleration, M is the mass of the trolley; $s_m(t)$ is the acceleration and m is the mass of the payload; l is the rope length, b is the viscous friction coefficient and $\theta(t)$ is the oscillation angle.

In order to simplify the modeling complexity, various assumptions will be made.

- The payload is connected to the trolley by a massless, rigid rope.
- The trolley and the bridge move along the track without slipping.
- The speed control system is assumed to be ideal, that is the actual speed is assumed to be equal to the reference one.
- The moment of inertia of the load is neglected, and it is treated as a point mass (notice that this approximation is valid also in case of a multi-wire rope [9])

The model can be deduced using the Eulero–Lagrange equations of motion:

$$\frac{d}{dt} \frac{\delta L}{\delta \dot{q}_k} - \frac{\delta L}{\delta q_k} = \tau_k; k = 1 \dots n$$

$$L = \frac{1}{2} \cdot (M + m)\dot{x}^2 + \frac{1}{2}ml^2\dot{\theta}^2 + ml\dot{x}\dot{\theta} \cos \theta + mgl \cos \theta \tag{1}$$

where $L = T - V$ is the Lagrangian of the system, defined as the difference between the kinetic and the potential energy, n is the number of degrees of freedom (DOF) of the system, $\{q_1 \dots q_n\}$ are a set of generalised coordinates and $\{\tau_1 \dots \tau_n\}$ represents a set of generalised force associated to the coordinates. In bridge cranes, the speed is controlled by the operator, so we consider $q = \theta$. The only external force related to the oscillation angle is the viscous friction, so $\tau = b\dot{\theta}$ where b is the friction coefficient. Solving Eq. (1), the equation of motion

$$\ddot{\theta}(t) = -\frac{1}{l} \left(\ddot{X}(t) \cos \theta(t) + g \sin \theta(t) + \frac{b}{ml} \dot{\theta}(t) \right) \tag{2}$$

is obtained. Linearizing the system about $\dot{\theta} = 0$, $\theta = 0$ and $u = 0$,

$$\frac{\theta(s)}{\ddot{X}(s)} = G(s) = \frac{-\frac{1}{l}}{s^2 + \frac{b}{ml^2}s + \frac{g}{l}} \tag{3}$$

is obtained, that is the relationship between the acceleration and the angle. Since the input of the system is the speed of the trolley (the motors are controlled using an inner speed control loop), we obtain

$$\frac{\theta(s)}{\dot{X}(s)} = F(s) = \frac{-\frac{1}{l}s}{s^2 + \frac{b}{ml^2}s + \frac{g}{l}} \tag{4}$$

3.1. Identification

On the basis of the model previously deduced, some tests have been carried out with the aim of identifying the parameters of the model.

Eq. (4) can be rewritten in the following form and the main parameters can be isolated:

$$F(s) = \frac{\theta(s)}{\dot{X}(s)} = \frac{\mu \cdot s}{D_2s^2 + D_1s + 1}$$

$$\mu = -\frac{1}{g}, D_1 = \frac{b}{mlg}, D_2 = \frac{l}{g} \tag{5}$$

A fixed delay introduced by the motor, as discussed in Section 2.1, is also introduced. The nominal value of this delay is set to 250 ms.

The identification tests have been made at different length of the rope and with various loads. In particular the rope length spans from one to six and a half meters, while two different loads were used, one of 600 Kg and the other of 5000 Kg (the hook by itself weighs 60 Kg).

The bridge crane was excited moving it backwards for 10 s and, after a delay, moving forward for other 10 s. Both the movements were made at the maximum speed reachable by the bridge crane.

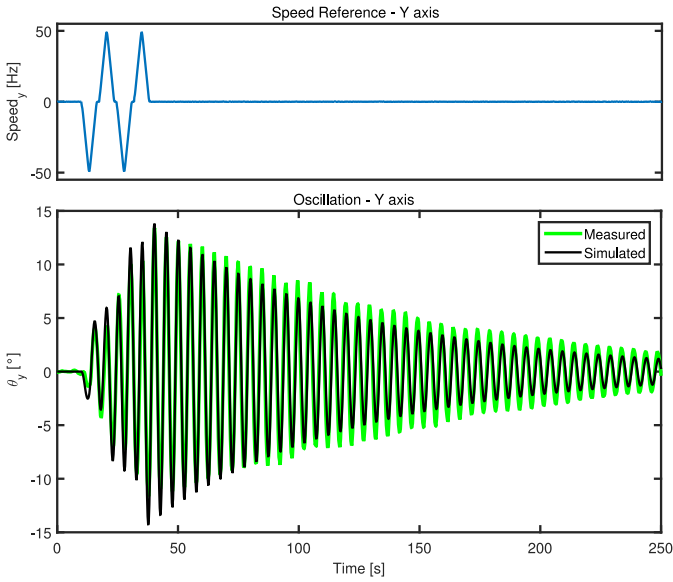


Fig. 6. Validation of the model identified on the Y axis. The rope length is 5 m with no load.

Table 1
Normalized root mean square index for all the identified models.

Rope length [m]	NRMSE [%]
1	39.73
2	59.02
3	67.09
4	77.50
5	82.92
6.5	77.59

In order to identify the optimal parameters of the model, the difference between the real data and the output of the simulation of the model described in Eq. 5 has been minimized. In particular, the cost function

$$J = \sum_{t=0}^N (\theta_{real}(t) - \theta_{sim}(t))^2 \quad (6)$$

is taken into consideration, where θ_{real} is the acquired angle, θ_{sim} is the simulation of the model and N is the number of available data.

The model identified for each value of l has been then validated in open loop. The tests have been made moving the bridge crane with a different path but with the corresponding rope length and load. The result of the validation for one of the models, is visible in Fig. 6.

In order to analyze the effectiveness of the identification, the *NRMSE* (*Normalized Root-Mean Square Error*) fitness value has been used as

$$NRMSE = 100 \cdot \left(1 - \frac{\|\theta_{real} - \theta_{sim}\|}{\|\theta_{real} - \text{mean}(\theta_{real})\|} \right). \quad (7)$$

The average *NRMSE* fitness index is 67.3, with the value for each model summarized in Table 1.

3.2. Sensitivity analysis

The bridge crane, due to its typical work-cycle, changes the rope length and the mass of the load very often. In detail, a typical work cycle is characterized by a connection of a load, a lift, a movement, a descent and a disconnection. It is clear that the mass of the load

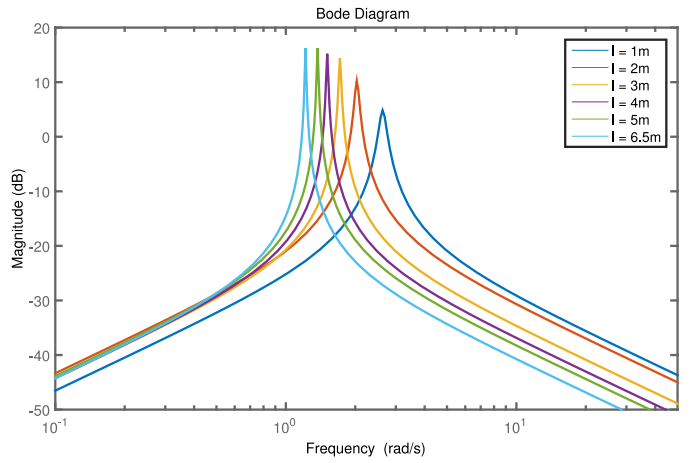


Fig. 7. Bode magnitude plots of the system with variation of the rope length. The mass was fixed at 60 Kg, while the rope length varies from 1 to 6.5 m.



Fig. 8. Bode magnitude plots of the system with variation of the load mass. The rope length was fixed at 5 m, while the load mass varies from 60 to 3000 Kg. A zoom on the resonance peak is also provided.

and the rope length frequently change. In Fig. 7, the bode diagrams of the models identified before, by varying the length of the rope and fixing the mass at 60 Kg, are shown. In Fig. 8, the same diagrams for fixed rope length of 5 m but different values of the mass are instead illustrated for a comparison.

The results confirms what can be obtained analyzing the second order model identified before. A rope length variation will significantly alter the bandwidth, the gain and the damping of the system, as visible in Fig. 7. The mass, instead, will cause only a slight change in the damping factor. For this reason, only the variation of the rope length will be considered in the design method.

In literature most of the approaches ([6], [20] and [13]) consider as scheduling variable the rope length. The previous analysis, with the fact that the rope length is the only measurements available of the two, strengthens the idea of creating a gain scheduling controller which changes its value depending on the length of the rope l . This parameter will become the scheduling variable.

4. Control design

In Section 3 the mathematical model of the bridge crane has been deduced emphasizing how the change of the rope length

heavily influences the system. For this reason a time invariant controller may have poor performance and even stability problems. The rope length has an important feature, that will be exploited in the design of the controller: it is decoupled in frequency with the band of the oscillations of the load.

4.1. Fixed-order gain-scheduling control design

The procedure used to design the controller is based on the methodology described in [12]; in order to tune the fixed-order linearly parameterized gain-scheduled controller a linear programming approach is used. The Nyquist diagram of the open-loop transfer function is shaped in order to respect some constraints which will guarantee lower bound on the robustness margin and optimal closed loop load disturbance rejection in terms of Integrated Error (IE):

$$IE = \int_0^\infty |e(t)|dt \tag{8}$$

where $e(t)$ is the difference between the desired output and the measured output.

The method guarantees the performance formulated before only in the frequency band used during the tuning of the controller. The closed-loop stability is locally ensured.

Defined the structure of the controller, the constraints on the robustness and performance, the problem is solved using an optimization algorithm which will find the best parameters for the controller. In particular, the linear programming problem has been solved using the CVX libraries ([8]).

4.1.1. Plant model

The method can be applied only to a particular class of SISO LPV systems: the plant model needs to depend on a n_l -dimensional vector l of scheduling parameters and must have no Right Half-Plane (RHP) poles. The dependence of the plant model from the scheduling parameter must be decoupled in frequency.

The definition of the n_l -dimensional vector will define a set of model, directly identified from the real plant. Suppose that this set covers all the range of values that can be assumed by the scheduling parameter and that it is available a sufficient amount of frequency points N to capture the dynamic of the systems; then the plant model can be parameterized in this manner:

$$\mathcal{M} = \{ \mathcal{F}(j\omega_k, l_i) \mid k = 1, \dots, N; i = 1, \dots, m \} \tag{9}$$

where ω_k is the vector of frequency for which the system will be evaluated and l_i is the vector of the scheduling parameter.

4.1.2. Controller definition

Consider the following class of controllers:

$$\mathcal{K}(s, l) = \rho^T(l)\phi(s) \tag{10}$$

with

$$\begin{aligned} \rho^T(l) &= [\rho_1(l), \rho_2(l), \dots, \rho_{n_p}(l)] \\ \phi^T(l) &= [\phi_1(l), \phi_2(l), \dots, \phi_{n_p}(l)] \end{aligned} \tag{11}$$

where n_p is the number of parameter ρ polynomially dependent from l and $\phi_i(s)$, $i = 1, \dots, n_p$ are rational basis functions with no RHP poles. The dependence of ρ_i on the parameter l can be represented using a polynomial of order p_c :

$$\rho_i(l) = (\rho_{i,p_c})^T l^{p_c} + \dots + (\rho_{i,1})^T l + (\rho_{i,0})^T \tag{12}$$

where l^k represent the element-by-element power of k of vector l . The controller can be completely defined using only the vectors of real parameters $\rho_{i,p_c}, \dots, \rho_{i,1}, \rho_{i,0}$.

Following the previous parametrization, a PID controller, with a quadratic dependence from the scheduling variable can be synthesized as follows:

$$\rho^T(l) = [K_p(l), K_i(l), K_d(l)] \tag{13}$$

$$\phi^T(s) = \left[1, \frac{1}{s}, \frac{s}{1+Ts} \right] \tag{14}$$

where T is the time constant of the noise filter; as said before, considering a second order dependence from the scheduling variable l , the controller parameters $\rho(l)$ are then:

$$\begin{aligned} K_p(l) &= K_{p,0} + K_{p,1}l + K_{p,2}l^2, \\ K_i(l) &= K_{i,0} + K_{i,1}l + K_{i,2}l^2, \\ K_d(l) &= K_{d,0} + K_{d,1}l + K_{d,2}l^2 \end{aligned} \tag{15}$$

The parametrization of the controller defined before associated with a set of non-parametric models, permits us to write every point of the Nyquist plot of the open-loop $L(j\omega, l_i) = \mathcal{K}(j\omega, l_i)\mathcal{F}(j\omega, l_i)$ as a linear function of the vector $\rho_i(l)$ ([14]):

$$\begin{aligned} \mathcal{K}(j\omega, l_i)\mathcal{F}(j\omega, l_i) &= \rho^T(l_i)\phi(j\omega)\mathcal{F}(j\omega, l_i) \\ &= \rho^T(l_i)\mathcal{R}(\omega, l_i) + j\rho^T(l_i)\mathcal{I}(\omega, l_i) \\ &= (M\bar{l}_i)^T \mathcal{R}(\omega, \bar{l}_i) + j(M\bar{l}_i)^T \mathcal{I}(\omega, \bar{l}_i) \end{aligned} \tag{16}$$

where

$$\begin{aligned} M &= \begin{bmatrix} (\rho_{1,p_c})^T & \dots & (\rho_{1,1})^T & (\rho_{1,0})^T \\ \vdots & \vdots & \ddots & \vdots \\ (\rho_{n_p,p_c})^T & \dots & (\rho_{n_p,1})^T & (\rho_{n_p,0})^T \end{bmatrix} \\ \bar{l}_i &= [l_i^{p_c} \dots l_i \bar{1}]^T, \end{aligned}$$

with $\mathcal{R}(\omega, l_i)$ and $\mathcal{I}(\omega, l_i)$ defined as the real and the imaginary part of $\phi(j\omega)\mathcal{F}(j\omega, l_i)$.

The system is now fully defined, and some optimization in terms of performance and robustness, can be performed.

4.1.3. Optimization for performance

Once the structure of the controller is defined, the optimization problem aims to find the controller parameters which are able to satisfy the following performance indexes:

- The system must remain stable for each variation, within a range, of the scheduling parameter. These constraints can be called *robustness constraints*.
- The Integrated Error (IE) must be reduced at its minimum. These constraints can be named *performance constraints*.

Solving the following minimization problem permits to satisfy the previous indexes:

$$\begin{aligned} \max_M \quad & K_{min} \\ \text{s.t.} \quad & (M\bar{l}_i)^T (\cot \alpha \mathcal{I}(\omega_k, l_i) - \mathcal{R}(\omega_k, l_i)) + K_r \leq 1 \\ & \forall \omega_k, \quad i = 1, \dots, m \\ & \sum_{j=1}^{n_p} \gamma_j \rho_j(l_i) - K_{min} \geq 0 \quad \text{for } i = 1, \dots, m \end{aligned} \tag{17}$$

where M is the matrix of the controller parameters and K_{min} is a term used to ensure the maximization of the low frequency part of the controller, represented by the term $k_0 = \sum_{j=1}^{n_p} \gamma_j \rho_j(l_i)$. The parameters γ_j allow to express k_0 as a linear combination of $\rho(l)$ in order to keep the formulation convex. For further details, see [10,12].

The design variables are K_r , which is linked to the gain margin value, and α , whose value is related to the phase margin (as described later in this Section). In Eq. (17), the first constraints are

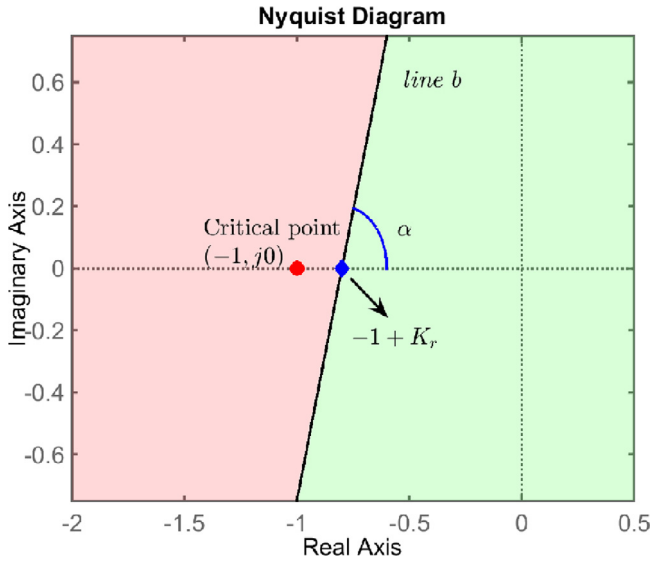


Fig. 9. Definition of the parameters used during the control design. The line b , defined by the parameter K_r and the angle α , divides the complex plane in two areas. The green area, below the line b is considered safe, while the red one, over the line b has to be avoided in order to keep the stability of the system. (For interpretation of the references to colour in this figure legend, the reader is referred to the web version of this article.)

related to the robustness performance, while the second type defines a constraint on the performance. Notice that the performance constraints focus on disturbance rejection, which is our goal. For this reason, the low-frequencies components of the controller have to be maximized ([2]).

The robustness constraints guarantee that the Nyquist plot of the open loop system will be below a line b that divide the complex plane in two regions, as visible in Fig. 9. The line crosses the real axis in $-1 + K_r$ with $0 < K_r < 1$ and with an angular coefficient defined by the value of $\alpha \in [0^\circ 90^\circ]$.

Ensuring that the Nyquist contour will be below the line b has the same meaning of ensuring that the open loop Nyquist plot will not encircle the critical point $(-1, j0)$. In this manner, exploiting the Nyquist criterion ([16]), it is possible to assure asymptotic stability against slow variation of the scheduling parameter.

Furthermore, placing the Nyquist curve of the open-loop transfer function on the right side of b , ensures lower bounds on conventional robustness margins ([10]):

$$G_m \geq \frac{1}{1 - K_r} \quad (18)$$

$$\phi_m \geq \arccos \left((1 - K_r) \sin^2 \alpha + \cos \alpha \sqrt{1 - (1 - K_r)^2 \sin^2 \alpha} \right) \quad (19)$$

$$M_m \geq K_r \sin \alpha \quad (20)$$

Where G_m , ϕ_m and M_m are the gain margin, the phase margin and the modulus margin.

As said before, α and K_r , are the design variables of the controller and their values highly influence the system performance. A wise decision of their values will be subject to discussion.

Analyzing the maximization problem presented in (17), it appears that the number of constraints depends on the frequency points ω and on the range of the scheduling parameter. Due to that, in order to solve the problem these two variables must be bounded. In particular, the problem related to the scheduling pa-

rameter is easy to solve since it is obvious that the set of non-parametric models available defines the length of the vector l_i .

The problem related to the frequency points, by the way, it is still unresolved since they are infinite. A solution to that is gridding the frequency domain: first, the band of the system must be analyzed, and then in that band, a finite number of equally spaced points are taken, making the number of constraints finite. Notice that the best discretization of the frequency axis is a trade-off choice between computational load and accuracy. However, this choice is strongly depending on the shape of the frequency response of the system and a general rigorous way to grid the frequency axis is subject of ongoing research.

4.2. Tuning of α

As described in Section 4.1.3, α is the angle by which, the line b , crosses the real axis defining the area where the Nyquist plots have to be. The value of this parameter has a relevant role inside the tuning of the controller, leading to an increment or decrement of the performance.

The other design variable, K_r is directly connected to the gain margin of the closed loop system by Eq. (18). Once this performance index is fixed, the others (module margin and phase margin) can be decided and consequentially even the value of α can be chosen. Instead of maximizing the phase margin, our approach is different: it is important to remove the sway as fast as possible, even permitting overshoot in the angle. For this reason it has been decided to fix the gain margin in order to obtain a robust controller and then compute the value of α by minimizing the time response to the sway disturbance. Summarizing, the following procedure is adopted.

1. Grid the parameter α within its range;
2. Tune a controller for each value of α by solving the constrained optimization problem (17);
3. Evaluate the settling time t_s of the closed-loop system for each α , where t_s is defined as the time elapsed from the application of an ideal instantaneous step input to the instant at which the output has entered and remained within a symmetric error band of 5%.
4. Choose the α which minimizes the mean of the settling time t_s (over the scheduling parameter l)

$$J_\alpha = \frac{1}{n_l} \sum_{i=1}^{n_l} t_s(\alpha, l_i)$$

An alternative to the minimization of the mean of the obtained settling times is the minimization of the worst case. In that sense, the following cost could be used in place of J_α :

$$V_\alpha = \max_i t_s(\alpha^{(i)}).$$

5. Results

In this section the results achieved on the real bridge crane will be presented. Firstly two different controller tuning processes will be presented and then, the tuned controllers will be tested on the real system.

5.1. Controller tuning

The method used for the tuning of the controller described in Section 4 is here applied on the real system. In particular, two different type of controller will be tuned. The first one will be tuned using the model of the system only at $l = 4.5$ m while the second one will be tuned knowing all the models connected to the variation of the scheduling parameter l .

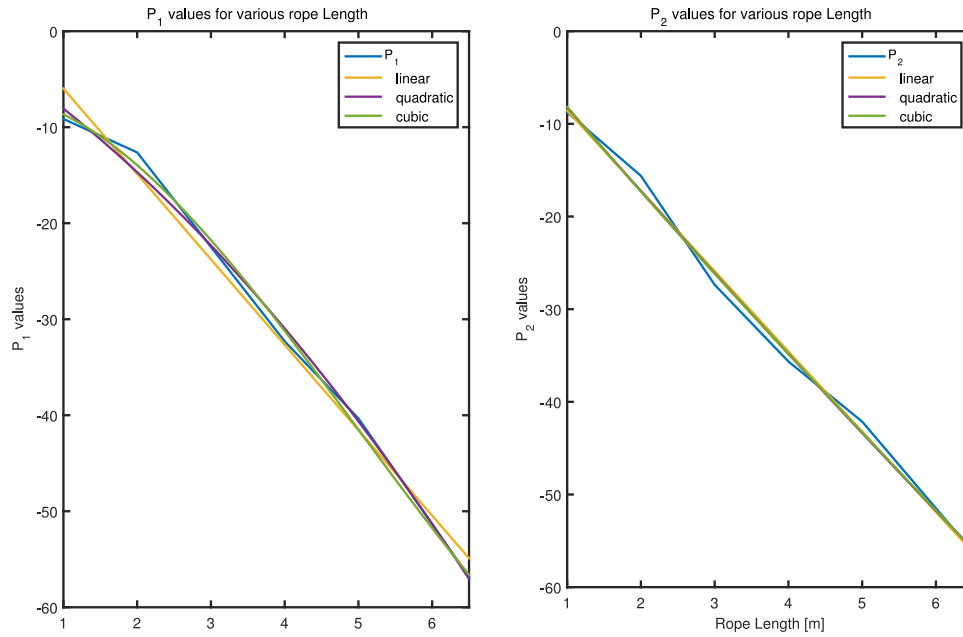


Fig. 10. The best P_1 (left) and P_2 for fixed values of l . The figure shows that a linear interpolation is good but a quadratic one is slightly better. A cubic interpolation is instead uselessly complicated.

The controller structure has been defined as

$$\mathcal{K}(s, l) = P_1(l) \frac{1}{1 + Ts} + P_2(l) \frac{s}{1 + Ts} \quad (21)$$

where P_1 and P_2 have a quadratic dependence on the scheduling parameter l :

$$P_i(l) = P_{i,2}l^2 + P_{i,1}l + P_{i,0} \quad i = 1, 2 \quad (22)$$

The selected structure arises from various considerations about the aim of the controller and the model of the system. Firstly the controller was chosen without a pure integral part since the cancellation with the derivator in the transfer function may hide some unstable behavior. For this reason a pole in low frequency has been added; the same pole increase even the gain at low frequency of the controller, increasing the disturbance rejection. The zero was added to increase the phase of the system; at the end the controller has a relative degree equal to zero, avoiding the introduction of delay in the loop.

Moreover, recall that the bridge crane is a differentially flat system that can be stabilized by a dynamic feedback controller when the input is the crane speed [11]. It turns out that the control signal needs to contain at least one integrator, which corresponds to our a-priori assumption on the controller structure.

In order to choose the correct dependence of the controller parameter from l , an LTI controller has been tuned for six different values of the length. From Fig. 10, it is clear that a quadratic dependence accurately captures both the mappings of P_1 and P_2 at different lengths.

The only parameter that must be chosen for the tuning of the controller is K_r . For a real-world application the recommended gain margin is at least 5 dB, leading to a $K_r = 0.8$ from Eq. (18). However, as it can be easily checked by simulations, this value of K_r leads to poor performance. A better trade-off between robustness and performance is instead $K_r = 0.2$, which is then set as design parameter.

5.1.1. Time invariant controller - K_{TI}

The time invariant controller, as the name explains, does not have a dependence from the scheduling parameter l . In fact its parameters depends only from the model identified at $l = 4.5$ m.

For this reason, the controller structure presented in Eq. (21) is changed, removing the dependency from l :

$$\mathcal{K}(s) = \bar{P}_1 \frac{1}{1 + Ts} + \bar{P}_2 \frac{s}{1 + Ts}. \quad (23)$$

Using the method described in 4 the controller does not guarantee robustness and optimal performance for all the variation of l , but only for $l = 4.5$ m. This should lead to loss of performance for the other value of the scheduling parameter.

The bridge crane used for the tests has a rope length which spans from 1 to 6.5 m, leading to a frequency bandwidth going from 0.19 Hz to 0.49 Hz. For this reason the frequency limits has been set from 0.01 Hz to 10 Hz, gridded every 0.001 Hz, leading to 9991 frequency points.¹ During the tuning of this controller, only one model has been used, the one identified during the test with the rope length set at 4.5 meters.

The gain margin K_r , has been set equal to 0.2, while the other design variable, α , as described in 4.2, has been tuned evaluating the step response time; in particular the best performance were achieved at $\alpha = 80^\circ$. These values lead to a bound in the gain margin of 1.25 and a phase margin of 28° . To be noticed that these values are valid only for the controller tuned at 4.5 m. The controller parameters obtained are the following:

$$\bar{P}_1 = -2.704, \quad \bar{P}_2 = -9.882 \quad (24)$$

In Fig. 11 it is shown the Nyquist diagrams of the open-loop system with the previously computed controller. In particular the Nyquist contour is presented for different rope lengths: from 1 to 6.5 m. As understandable, since during the tuning phase only the model at 4.5 m has been considered, the constraints related to performance and robustness may not be respected. In particular it is clear how the Nyquist contour exceeds the line b in 4 of the 6 different models (without considering the one at 4.5 m). More in deep, the controller for the model at one and two meters pushes the Nyquist diagram to rotate around the critical point $(-1, j0)$ making the closed loop system unstable.

¹ Note that a logarithmically spaced frequency grid instead of an equidistant gridding could be equivalently used. In this case, no particular differences in performance can be shown.

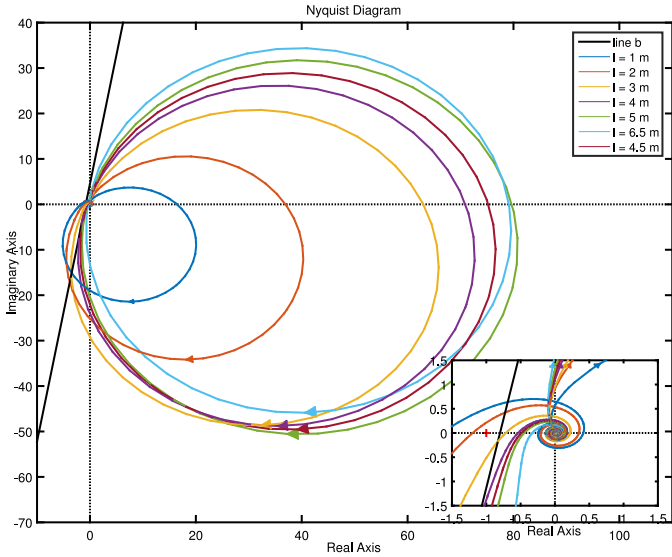


Fig. 11. Nyquist plots of the open loop system with the K_{TI} controller. The stability is guaranteed only for $l = 4.5\text{m}$; in fact the system with this rope length is below the line b , while for other length, like for example 1, 2, 3 and 4 meter the Nyquist contours is over the line. This does not mean that the system is unstable.

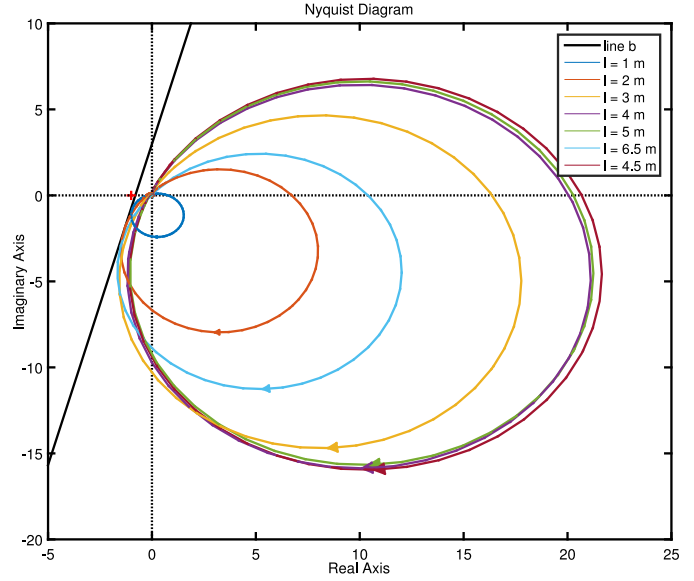


Fig. 13. Nyquist plots of the closed loop system with the gain scheduling controller. It is visible how all the contours, varying the rope length l , remain below the line b .

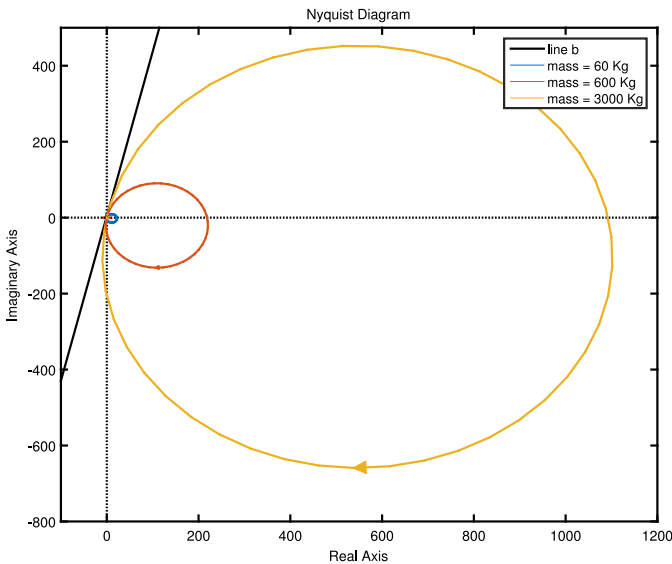


Fig. 12. Nyquist plots of the open loop system with the K_{TI} controller, at 4.5 m, with different masses connected. The change of the load mass influences only the resonance peak of the system, and consequentially, only the radius of the Nyquist contour.

With the K_{TI} controller, a test has been carried out in order to evaluate the effects of a change in the load mass. In Fig. 8 it is possible to see that a change in the mass influences the resonance peak of the model; analyzing the same parameter variation in the system with the K_{TI} controller, it is possible to see how the mass will influence only the *radius* of the Nyquist contour, which is directly connected to the resonance peak, as visible in Fig. 12. As a consequence, for the considered system, a change in the mass will not create problem in terms of stability or loss of performance; this, with the motivations described in Section 3.2, confirms that scheduling the controller on the rope length is a wise choice.

5.1.2. Gain scheduling - K_{GS}

The gain scheduling has been tuned exploiting six different identified model at different rope length. In particular the rope

length varied from 1 to 6.5 with 6 almost equispaced steps. The controller has the same structure of the one described in Sections 5.1.1 and 4. The two parameters of the controller have a quadratic dependence on the scheduling parameter.

The frequency band is the same of the K_{TI} controller, so the number of constraints related to the robustness index for each rope length is still the same, 9991. The difference here is that, instead of only one scheduled parameter, there are 6 different values of the parameter. This leads to $9991 \cdot 6 = 59,946$ constraints. The other type of constraints, the performance ones, are related only to the number of values assumed by the scheduling parameter, so only 6, leading to a total number of 59,952 constraints.

The optimization problem leads to the following controller parameters:

$$\begin{aligned}
 P_1(l) &= -0.004 \cdot l^2 + 0.016 \cdot l - 2.66 \\
 P_2(l) &= 0.433 \cdot l^2 - 3.338 \cdot l + 1.451
 \end{aligned}
 \tag{25}$$

These parameters were obtained with an $\alpha = 75^\circ$, which permits to minimize the step response time, and a $K_r = 0.2$. These values permits to have a gain margin equal to 1.25 and a phase margin of around 24.4° . Notice that the value of α employed here is different from that used for the time-invariant controller in the previous subsection. This is due to the fact that the selection rule is the same but the two controllers refer to two different plants: one considering all possible values of l and the other considering only the nominal value of l . These indexes are lower bound for all the different values assumed by the scheduling parameter l . With the controller obtained, as visible in Fig. 13, all the Nyquist plots for different rope lengths are in the safe are, below the line b defined by the parameters α and K_r .

In Fig. 14, the step response of the K_{TI} controller, the K_{GS} controller and the system without control are shown. It can be observed that the K_{TI} controller, at its tuning point 4.5 m, has better performance, in terms of response time, compared to the gain scheduling controller.

At six meter the time invariant controller still have better performance compared to K_{GS} , but the performance loss in the Gain Scheduling case is due to the high level of robustness requested, which is not insured by K_{TI} . In the three meter case instead, the damping of the sway is more similar. To be remembered that the

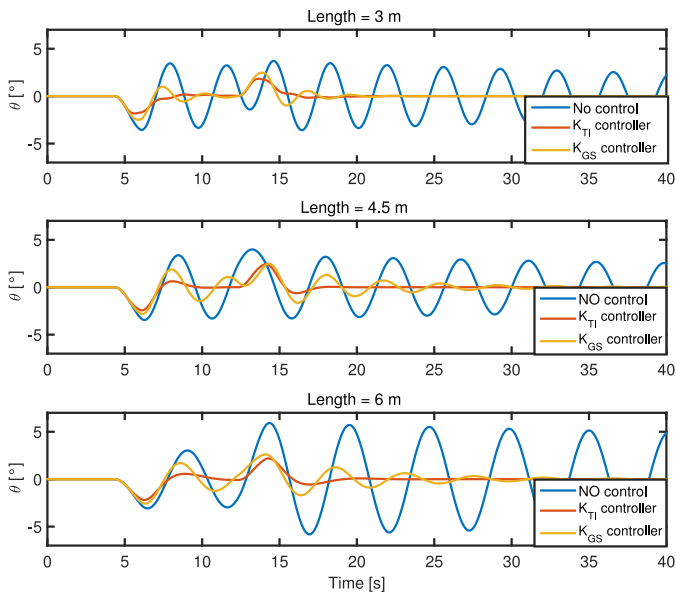


Fig. 14. Simulation results of a step response of the closed loop system without control, with the time invariant and with the gain scheduling controller. The results are shown for three different rope length.

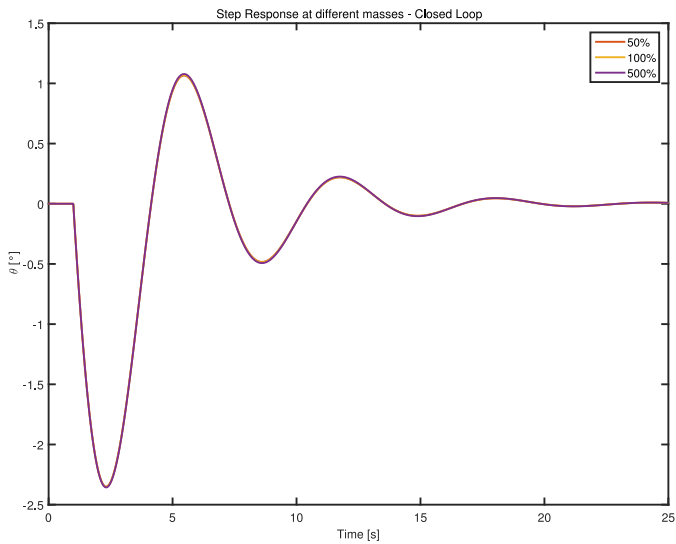


Fig. 15. Closed-loop step responses with different values of the load. This test further validates that the change of the mass can be neglected in the design of the controller.

K_{Tl} controller is not able to guarantee the stability of the closed loop system in all the conditions. At one and two meters the system is unstable, leading to unusability of the controller in a real environment.

The closed-loop simulator can be used also to finally validate the fact that the mass variation can be neglected in the GS controller design. In fact, from Fig. 15, which shows the closed-loop step responses corresponding to different values of the load, it is evident that the system with very different masses has practically the same behavior.

5.2. A comparison with state of the art tools

One may think to track the operator speed reference signal together with the zero sway angle, instead of letting the operator command in open loop. Therefore, in this subsection, the proposed method is compared with a second control scheme, where

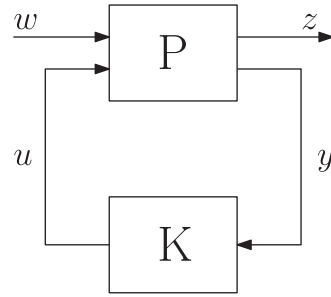


Fig. 16. The feedback control architecture for `hinfgs` design.

both the operator speed reference and the zero load oscillation are tracked.

More specifically, the feedback control architecture shown in Fig. 16 is employed, where

- w is the collection of the reference signals, i.e. the input of the operator and the zero reference angle;
- z describes the performance indexes, that include the error between the reference speed and the actual speed and the error between the reference angle and the measured angle;
- y is the output of the system (used as input of the controller). In this case, $y = z$ is selected;
- u is the control variable of the system, namely the motor command input;
- P is the plant, the bridge crane;
- K is a H_∞ gain scheduling controller.

To provide a fair comparison, the H_∞ gain scheduling controller is tuned by means of the well established Matlab tool `hinfgs` following the method in [1].

The responses of speed and sway angle using the above scheme and the proposed fixed-order controller are shown in the simulations of Fig. 17. From the results, it can be seen that the H_∞ gain scheduling controller clearly outperforms the proposed one as far as speed tracking is concerned (the step responses have no overshoot for any value of the length). Instead, concerning closed-loop sway dynamics, the H_∞ gain scheduling controller performs generally slightly better, but the worst case ($l = 1\text{ m}$) is worse than with the proposed fixed order controller. Moreover, notice that the proposed controller makes the system response almost constant for all the interesting values of the length. This means that the system behaviour with the proposed solution is repeatable and more easily predictable, thus making the interaction with the operators more safe.

Nonetheless, the controller provided by `hinfgs` turns out to be a 4th order controller (thus of higher order than the proposed one) and requires the knowledge of the mass of the cart for its design as well as the availability of the measurement of the speed of the bridge crane. Notice that, in many existing bridge cranes, the speed measurement is not available and the mass value is difficult to recover accurately.

To conclude, although both the design strategies seem good for the considered control purpose, the best choice between them is not obvious and depends on system limitations, performance requirements and controller complexity. In some specific situations, e.g. if the speed sensor is not available, the proposed solution is the only applicable one.

5.3. Experimental results

On the bridge crane described in Section 2.1, some tests have been carried out, in order to evaluate the performance of the two

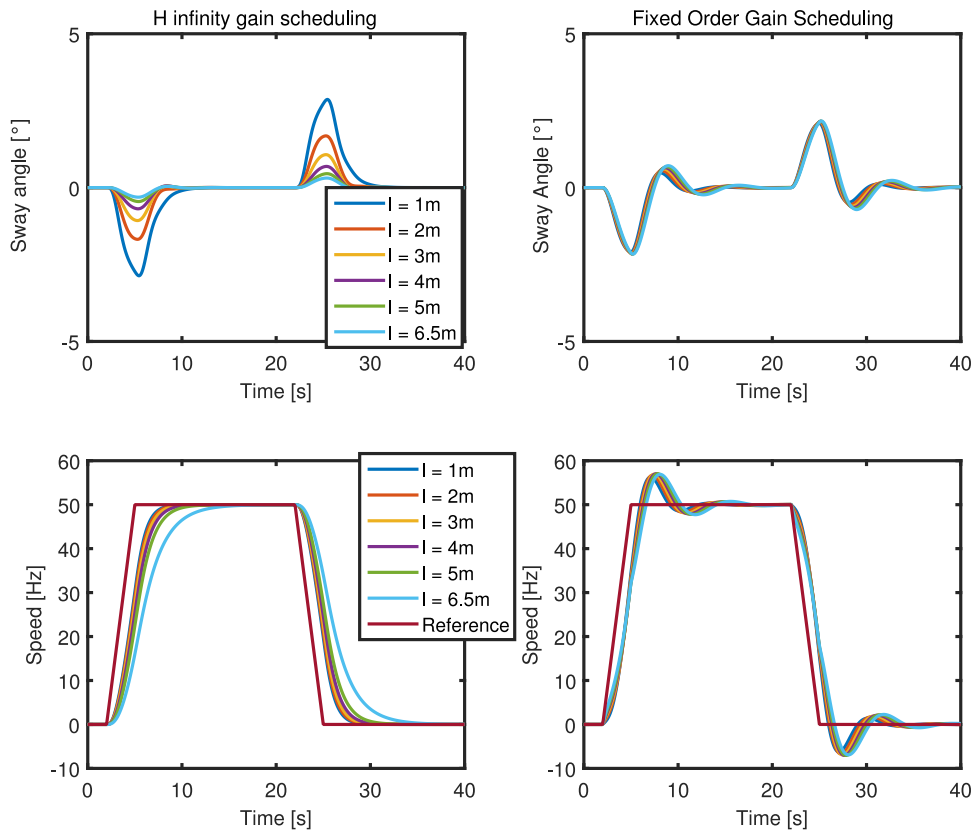


Fig. 17. Closed-loop performance with the proposed controller (right) and the H_∞ gain scheduling controller tuned via `hinfgs` (left).

controllers previously designed. In particular the aim was to evaluate the effectiveness of the gain scheduling controller compared to the time invariant one. To do this, three tests at different rope length, were made:

- Test 1: step response of the system with a rope length of 3 m;
- Test 2: step response of the system with a rope length of 4.5 m;
- Test 3: step response of the system with a rope length of 6 m;

The input of the system, in these three tests, is not a real step, since it is physically impossible to implement a real step on a mechanical system like the bridge crane. Due to the high inertia and to some structural limitations it was possible to use as input only a ramp that reach the maximum speed in 1 s. Higher accelerations introduce slipping of the wheel on the track, and excite the non-linear behavior of the system.

All the tests were made without any load connected and moving the bridge crane only on the y axis.

The results of these tests can be seen in Fig. 18; in particular in the top figure it is visible the *Test 1*, in the middle the *Test 2* and the bottom figure is the *Test 3*. These results show the effectiveness of the gain scheduling controller, which is able to attain the aim of reducing the sway of the load in all the conditions.

The controller has been digitalized using Tustin and a working frequency of 100 Hz and then implemented on a PLC (Programmable Logic Controller).

The performance has been evaluated computing the RMS error; the values of this index are shown in Table 2 for each type of controller.

5.4. Discussion

The Fig. 18 confirms the results achieved with the controller. In particular the introduction of the gain scheduling controller per-

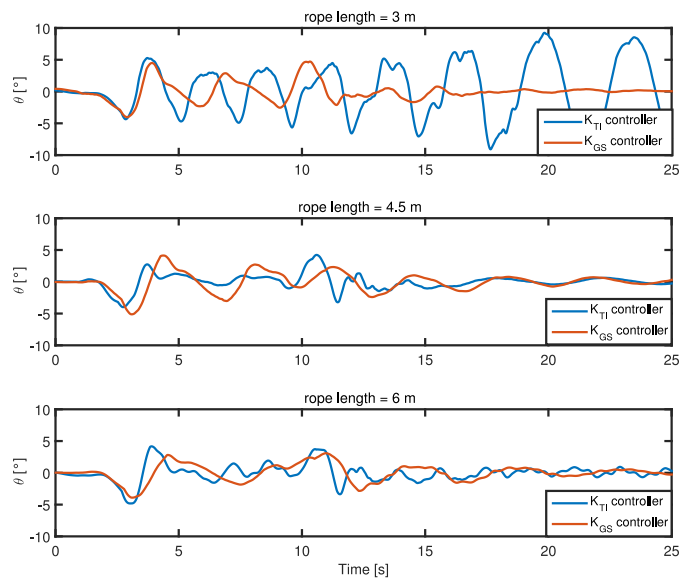


Fig. 18. Real tests made on the bridge crane. The results are shown for the system with the time invariant controller and with the gain scheduling controller, for three different rope length.

mits to maintain an high level of performance in terms of assessment time. Further more the K_{GS} controller is more robust compared to the K_{TI} one; in fact in the *Test 1* the system become unstable with the K_{TI} controller. This is due to differences between the real model and the mathematical one. The uncertainty with the largest issue is related to the delay; in fact it is not fixed, its value changes even in the same condition.

Table 2

Root mean square error, in degree, of the oscillation angle compared with the desired one. This index is shown for the two different type of control.

Rope length [meter]	RMS Error [°]	
	Nominal	GS
3	4.89	1.49
4.5	1.23	1.32
6	1.40	1.38

Different tests showed that the delay may vary from 190 up to 290 ms. Notice that the delay influences the phase margin of the system. Since the GS controller ensures a lower bound on this parameter (in our case 24°), the system with such a controller is also more robust to possible variation of the delay. The K_{TI} controller ensures the same lower bound on the phase margin only at 4.5 m, while in the other cases, a change in the delay decreases the phase margin. It follows that, with the LTI controller, in the worst case the stability of the closed loop system is not even guaranteed.

These results are confirmed by the RMS error, which shows a similar value for K_{TI} and K_{GS} with a rope length of 4.5 m and 6, while for the case of 3 m the gain scheduling has better performance. The RMS error is resumed in Table 2.

6. Conclusions

In this paper, the problem of sway reduction in bridge cranes is tackled. To this aim, a fixed-order gain scheduling controller is designed, with the aim of being robust with respect to unmodeled dynamics and maximizing the speed performance. The original tuning method has been extended by adding a performance oriented tuning of α and the resulting controller has been experimentally validated and compared with a time-invariant law tuned according to the same specifications and with a state of the art tool for gain scheduling design.

The proposed control algorithm, thanks to its low computational burden, can be implemented on a low cost hardware, thus permitting to improve the performance of existing bridge cranes.

Future work will be devoted to LPV control of bridge cranes for fast load lifting.

References

- [1] Apkarian P, Gahinet P, Becker G. Self-scheduled h-infinity control of linear parameter-varying systems: a design example. *Automatica* 1995;31(9):1251–61.
- [2] Åström KJ, Hägglund T. *Advanced PID control*. ISA-The Instrumentation, Systems, and Automation Society; Research Triangle Park, NC 27709; 2006.
- [3] Auernig J, Troger H. Time optimal control of overhead cranes with hoisting of the load. *Automatica* 1987;23(4):437–47.
- [4] Bartolini G, Pisano A, Usai E. Second-order sliding-mode control of container cranes. *Automatica* 2002;38(10):1783–90.
- [5] Comotti D, Ermidoro M, Galizzi M, Vitali A. Development of an attitude and heading reference system for motion tracking applications. In: *Sensors and Microsystems*. Springer; 2014. p. 335–9.
- [6] Corrigan G, Giua A, Usai G. An implicit gain-scheduling controller for cranes. *Cont Syst Technol, IEEE T* 1998;6(1):15–20.
- [7] Ermidoro M, Formentin S, Cologni A, Previti F, Savaresi SM. On time-optimal anti-sway controller design for bridge cranes. In: *American Control Conference (ACC)*, 2014. IEEE; 2014. p. 2809–14.
- [8] Grant M., Boyd S. CVX: Matlab software for disciplined convex programming, version 2.1. <http://cvxr.com/cvx>; 2014.
- [9] H Lee YL, Segura D. A new approach for the anti-swing control of overhead cranes with high-speed load hoisting. *Int J Control*, 2003;76(15):1493–9.
- [10] Karimi A, Kunze M, Longchamp R. Robust controller design by linear programming with application to a double-axis positioning system. *Cont Eng Pract* 2007;15(2):197–208.
- [11] Kolar B, Schlacher K. Flatness based control of a gantry crane. In: *IFAC Symposium on Nonlinear Control Systems*; 2013. p. 487–92.
- [12] Kunze M, Karimi A, Longchamp R. Gain-scheduled controller design by linear programming with application to a double-axis positioning system. *Tech. Rep. Institute of Electrical and Electronics Engineers*; 2009.
- [13] Lee H-H. Modeling and control of a three-dimensional overhead crane. *J Dyn Syst, Measure, Cont* 1998;120(4):471–6.
- [14] Leith DJ, Leithead WE. Survey of gain-scheduling analysis and design. *Int J Cont* 2000;73(11):1001–25.
- [15] Liu D, Yi J, Zhao D, Wang W. Adaptive sliding mode fuzzy control for a two-dimensional overhead crane. *Mechatronics* 2005;15(5):505–22.
- [16] Nyquist H. Regeneration theory. *Bell Syst Tech J* 1932;11(1):126–47.
- [17] Piazza A, Visioli A. Optimal dynamic-inversion-based control of an overhead crane. *IEE Proc-Cont Theory App* 2002;149(5):405–11.
- [18] Singer N, Singhose W, Kriikku E. An input shaping controller enabling cranes to move without sway. In: *ANS 7th topical meeting on robotics and remote systems*, 1; 1997. p. 225–31.
- [19] Sorensen KL, Singhose W, Dickerson S. A controller enabling precise positioning and sway reduction in bridge and gantry cranes. *Cont Eng Prac* 2007;15(7):825–37.
- [20] Zavari K, Pipeleers G, Swevers J. Gain-scheduled controller design: illustration on an overhead crane. *Ind Electron, IEEE T* 2014;61(7):3713–18.